

## Crystallization of bastnäsite and burbankite from carbonatite melt in the system La(CO<sub>3</sub>)F-CaCO<sub>3</sub>-Na<sub>2</sub>CO<sub>3</sub> at 100 MPa

ANNA M. NIKOLENKO<sup>1,2,3,\*</sup>, KONSTANTIN M. STEPANOV<sup>3,4</sup>, VLADIMIR RODDATIS<sup>1</sup>, AND  
ILYA V. VEKSLER<sup>1,3,†</sup>

<sup>1</sup>Helmholtz Centre Potsdam—German Research Centre for Geosciences GFZ, Telegrafenberg, 14473 Potsdam, Germany

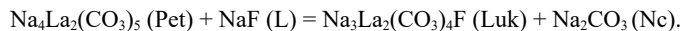
<sup>2</sup>University of Potsdam, Institute of Geosciences, Karl-Liebknecht-Str. 24-25, 14476 Potsdam-Golm, Germany

<sup>3</sup>V.S. Sobolev Institute of Geology and Mineralogy SB RAS, Akad. Koptuyuga, 3, Novosibirsk 630090, Russia

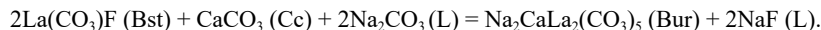
<sup>4</sup>Vereshchagin Institute for High Pressure Physics RAS, Troitsk, 142190 Moscow, Russia

### ABSTRACT

Bastnäsite [REE(CO<sub>3</sub>)F] is the main mineral of REE ore deposits in carbonatites. Synthetic bastnäsite-like compounds were precipitated from aqueous solutions by many different methods, but previous attempts to model magmatic crystallization of bastnäsite from hydrous calciocarbonatite melts were unsuccessful. Here we present the first experimental evidence that bastnäsite and two other REE carbonates, burbankite, and lukechangite, can crystallize from carbonatite melt in the synthetic system La(CO<sub>3</sub>)F-CaCO<sub>3</sub>-Na<sub>2</sub>CO<sub>3</sub> at temperatures between 580 and 850 °C and a pressure 100 MPa. The experiments on starting mixtures of reagent-grade CaCO<sub>3</sub>, Na<sub>2</sub>CO<sub>3</sub>, La<sub>2</sub>(CO<sub>3</sub>)<sub>3</sub>, and LaF<sub>3</sub> were carried out in cold-seal rapid-quench pressure vessels. The studied system is an isobaric pseudoternary join of a quinary system where CO<sub>2</sub> and fluorides act as independent components. Liquidus phases in the run products are calcite, nyerereite, Na carbonate, bastnäsite, burbankite solid solution (Na,Ca)<sub>3</sub>(Ca,La)<sub>3</sub>(CO<sub>3</sub>)<sub>5</sub>, and lukechangite Na<sub>3</sub>La<sub>2</sub>(CO<sub>3</sub>)<sub>4</sub>F. Calcite and bastnäsite form a eutectic in the boundary join La(CO<sub>3</sub>)F-CaCO<sub>3</sub> at 780 ± 20 °C and 58 wt% La(CO<sub>3</sub>)F. Phase equilibria in the boundary join La(CO<sub>3</sub>)F-Na<sub>2</sub>CO<sub>3</sub> are complicated by peritectic reaction between Ca-free end-member of burbankite solid solution petersenite (Pet) and lukechangite (Luk) with liquid (L):



The right-hand-side assemblage becomes stable below 600 ± 20 °C. In ternary mixtures, bastnäsite (Bst), burbankite (Bur), and calcite (Cc) are involved in another peritectic reaction:



Burbankite in equilibrium with calcite replaces bastnäsite below 730 ± 20 °C. Stable solidus assemblages in the pseudoternary system are: bastnäsite-burbankite-fluorite-calcite, bastnäsite-burbankite-fluorite-lukechangite, bastnäsite-burbankite-lukechangite, burbankite-lukechangite-nyerereite-calcite, and burbankite-lukechangite-nyerereite-natrite. Addition of 10 wt% Ca<sub>3</sub>(PO<sub>4</sub>)<sub>2</sub> to one of the ternary mixtures resulted in massive crystallization of La-bearing apatite and monazite and complete disappearance of bastnäsite and burbankite. Our results confirm that REE-bearing phosphates are much more stable than carbonates and fluorocarbonates. Therefore, primary crystallization of the latter from common carbonatite magmas is unlikely. Possible exceptions are carbonatites at Mountain Pass that are characterized by very low P<sub>2</sub>O<sub>5</sub> concentrations (usually at or below 0.5 wt%) and extremely high REE contents in the order of a few weight percent or more. In other carbonatites, bastnäsite and burbankite probably crystallized from highly concentrated alkaline carbonate-chloride brines that were found in melt inclusions and are thought to be responsible for widespread fenitization around carbonatite bodies.

**Keywords:** Experimental petrology, carbonatite melts, REE ore deposits, Mountain Pass, Bayan Obo

### INTRODUCTION

Mountain Pass in California, U.S.A., and Bayan Obo in China are the world's two largest deposits of rare earth elements (REE) associated with carbonatites, and bastnäsite REE(CO<sub>3</sub>)F is the main ore-forming mineral in both. Bastnäsite belongs to a

group of fluorocarbonates characterized by the general formula  $n \text{REE}(\text{CO}_3)(\text{F},\text{OH}) \cdot m \text{CaCO}_3$  where  $m = 0$  (bastnäsite), or 1 (synchisite, parisite, röntgenite), and  $n = 1$  (bastnäsite, synchisite), 2 (parisite), or 3 (röntgenite). The bastnäsite crystal structure is formed by REE-F layers parallel to the (001) plane with triangular carbonate (CO<sub>3</sub>)<sup>2-</sup> ions arranged between the layers. Other minerals of the group have layers of Ca<sup>2+</sup> ions alternating with the layers of REE-F (Donnay and Donnay 1953). In addition

\* E-mail: annanik@gfz-potsdam.de. Orcid 0000-0003-4731-9134

† Orcid 0000-0002-9692-363X

to Ca and REE, fluorocarbonates may contain major amounts of Na (arisite, lukechangite), Ba (cordylite, cebaite), and other alkaline earth elements. Giant bastnäsite deposits at Mountain Pass and Bayan Obo are hosted by very unusual carbonatites, but fluorocarbonates of the bastnäsite group are also quite common in classical carbonatites that are related to silica-undersaturated nephelinitic and melilititic magmas. In typical carbonatites, REE fluorocarbonates are often associated with mixed carbonates such as calcite, carbocelestite, ancylite, and the burbankite group minerals  $(\text{Na,Ca})_3(\text{Ca,REE})_3(\text{CO}_3)_5$  (Belovitskaya and Pekov 2004; Chakhmouradian and Zaitsev 2012; Zaitsev et al. 2002). Because carbonatites are usually strongly enriched in light rare earths, REE in minerals of the bastnäsite, and burbankite groups are mostly represented by Ce, La, Nd, and Pr (in this order of decreasing natural abundance) (Fleischer 1978; Williams-Jones and Wood 1992).

Since the first successful hydrothermal synthesis of bastnäsite in the 1950s (Jansen et al. 1959), hydroxy- and fluorobastnäsite compounds have been precipitated from aqueous solutions by different methods at atmospheric and elevated pressure (Wyllie and Tuttle 1960; Mercier et al. 1993; Haschke 1975; Hsu 1992; Pradip et al. 2013; Shivaramaiah et al. 2016). Interest in bastnäsite-type compounds has been growing in recent decades because of their use as starting materials for production of rare earth oxycarbonates ( $\text{REE}_2\text{O}_2\text{CO}_3$ ) and oxyfluorides (REEOF), which are excellent host matrices for phosphorus used in optical technologies (Janka and Schleid 2009; Lee and Jung 2013), and also for the production of  $\text{CeO}_2$  nanoparticles (Montes-Hernandez et al. 2016). According to Haschke (1975), synthetic  $\text{La}(\text{CO}_3)(\text{OH})$  loses  $\text{H}_2\text{O}$  and  $\text{CO}_2$  at ambient pressure between 425 and 525 °C to form  $\text{La}_2\text{O}_2\text{CO}_3$ , which subsequently decomposes to  $\text{La}_2\text{O}_3$  between 625 and 800 °C. Decomposition of synthetic  $\text{La}(\text{CO}_3)\text{F}$  at atmospheric pressure occurs between 520 and 550 °C with the formation of fluoroxide LaOF. Thermal stability of La-bastnäsite increases at  $P_{\text{CO}_2} = 100$  MPa to 810 °C for  $\text{La}(\text{CO}_3)(\text{OH})$  and 860 °C for  $\text{La}(\text{CO}_3)\text{F}$  (Hsu 1992). Experiments by Rowland (2017) and Rowland et al. (2020) showed that a further increase of pressure up to 1 GPa does not seem to significantly increase the thermal stability of  $\text{La}(\text{CO}_3)\text{F}$ , and the decomposition temperature remains between 850 and 900 °C.

In summary, bastnäsite-like compounds have been generally synthesized by different methods in hydrothermal experiments, but it has not been shown yet whether bastnäsite can crystallize from carbonate melt at conditions relevant for natural carbonatite magma. Jones and Wyllie (1983, 1986) and Wyllie et al. (1996) experimented on La-bearing carbonatite melts in the system  $\text{CaCO}_3\text{-Ca}(\text{OH})_2\text{-La}(\text{OH})_3$  at 100 MPa, but lanthanum hydroxide was the only La crystalline phase found in the run products. Wyllie et al. (1996) briefly mentioned that they had observed co-crystallization of calcite and hydroxybastnäsite from La-rich carbonatite melt in the system  $\text{CaCO}_3\text{-Ca}(\text{OH})_2\text{-La}(\text{CO}_3)(\text{OH})$  between 550 and 630 °C but a detailed account of the experiments has not been published. Experiments on more complex compositions in the system  $\text{CaCO}_3\text{-BaSO}_4\text{-CaF}_2\text{-Ca}(\text{OH})_2\text{-La}(\text{OH})_3$  were designed to model crystallization of carbonatitic melts that may have been parental to the Mountain Pass REE deposit (Jones and Wyllie 1986; Wyllie et al. 1996) also did not produce bastnäsite. Lanthanum hydroxide was again the only La phase stable at

temperatures up to 710 °C, and above that temperature it was replaced by oxyfluoride LaOF.

Notably, previous experimental studies universally used synthetic calciocarbonate melts with large amounts of  $\text{H}_2\text{O}$  to lower crystallization temperatures down to a geologically realistic level. However, a growing amount of geological and experimental evidence (Kjarsgaard 1998; Kjarsgaard et al. 1995; Nabyl et al. 2020; Weidendorfer et al. 2017) and studies of melt inclusions (Guzmics et al. 2015; Nielsen et al. 1997; Panina 2005; Sokolov et al. 1999; Veksler et al. 1998) imply that common carbonatite melts associated with nephelinitic and melilititic rocks contain variable but significant amounts of alkalis. Therefore, low-crystallization temperatures of natural carbonatitic melts, down to about 560–600 °C, are probably due to the presence of alkali carbonate components rather than  $\text{H}_2\text{O}$  alone. Concentrations of total alkalis ( $\text{Na}_2\text{O}+\text{K}_2\text{O}$ ) in carbonatite liquids at the start of magmatic crystallization of calcite are estimated to be somewhere between 5–20 wt% (Lee and Wyllie 1998; Weidendorfer et al. 2017), and fractional crystallization of calcite, apatite and minor silicates is expected to increase the alkali content in evolving carbonatite liquid up to 32–35 wt%, characteristic concentrations in natrocarbonatite lava (Gittins and Jago 1998; Weidendorfer et al. 2017). All this evidence implies that common calciocarbonatites should probably be interpreted as calcite cumulates that have lost significant amounts of alkalis (especially Na) to fenitizing fluids expelled from evolving carbonatite magma at advanced stages of crystallization (Rankin 2005 and references therein). Alkali loss from carbonatites has been documented by numerous field observations for many decades (e.g., von Eckermann 1966) and was tested experimentally (Veksler and Keppler 2000).

In summary, a realistic experimental model of natural carbonatite liquid derived from nephelinitic magma at crustal pressure should crystallize calcite as a primary liquidus phase but contain major amounts of alkali carbonate components. Here we present the first experimental evidence for crystallization of bastnäsite and burbankite solid solutions from carbonatite melt in the system  $\text{La}(\text{CO}_3)\text{F-CaCO}_3\text{-Na}_2\text{CO}_3$ . Lanthanum was chosen to represent REE because it is the second most abundant REE after Ce in carbonatites and, unlike the latter, has only one (trivalent) oxidation state that is most typical for rare earths. In addition, we performed a few pilot experiments on a four-component mixture containing 10 wt%  $\text{Ca}_3(\text{PO}_4)_2$ . The additional runs were done to study the effects of apatite and monazite crystallization on the stability of bastnäsite and burbankite. In the discussion, we draw some implications for the formation of REE deposits in carbonatites.

## EXPERIMENTAL AND ANALYTICAL METHODS

Starting mixtures were prepared from reagent-grade  $\text{CaCO}_3$ ,  $\text{Na}_2\text{CO}_3$ ,  $\text{La}_2(\text{CO}_3)_3$ ,  $\text{Ca}_3(\text{PO}_4)_2$ , and  $\text{LaF}_3$ . Pure reagents were dried at 100 °C overnight, mixed under acetone in agate mortar, and then dried again. First, we prepared an equimolar mixture of  $\text{La}_2(\text{CO}_3)_3$  and  $\text{LaF}_3$  that is equivalent to stoichiometric  $\text{La}_2(\text{CO}_3)\text{F}$  and then mixed it with various amounts of Na and Ca carbonates. We used 12 mixtures with concentrations of the  $\text{La}_2(\text{CO}_3)\text{F}$  component ranging from 20 to 50 wt%, including four binary mixtures  $\text{CaCO}_3\text{-La}_2(\text{CO}_3)\text{F}$  and  $\text{Na}_2\text{CO}_3\text{-La}_2(\text{CO}_3)\text{F}$  (see Table 1). We tried to keep our starting mixtures as dry as possible, but because we obtained  $\text{La}_2(\text{CO}_3)_3$  by controlled dehydration of a commercially produced (Sigma-Aldrich) crystal hydrate  $\text{La}_2(\text{CO}_3)_3 \cdot x\text{H}_2\text{O}$ , minor amounts of  $\text{H}_2\text{O}$  cannot be ruled out. Another potential source of  $\text{H}_2\text{O}$  in run products is hydrogen diffusion through gold and platinum container walls during the experiments (Brooker et al. 1998).

Experiments were conducted in rapid-quench cold-seal pressure vessels at the German Research Centre for Geosciences (GFZ Potsdam). A detailed description of this type of vessel was presented by Matthews et al. (2003). The autoclaves at GFZ Potsdam are made of the Ni-Cr alloy Vakumelt ATS 290-G (ThyssenKrupp AG). Temperature was measured by an external Ni-CrNi thermocouple calibrated against the melting temperature of gold. Total error of temperature measurements, including the uncertainties due to the temperature gradients, is estimated to be  $\pm 5$  °C. Pressure was measured by transducers, and the results were checked against a pressure gauge. The transducers and gauge were factory-calibrated and have an accuracy of better than  $\pm 0.1$  MPa. About 20–30 mg of starting materials were loaded into gold or platinum capsules, 3 mm in outer diameter and 15 mm in length. Quenching of samples was semi-isobaric and lasted a few seconds.

Run products were mounted in epoxy resin and polished using sandpaper and diamond polishing pastes without water to avoid dissolution of alkali carbonates and other water-soluble components. SEM images for preliminary identification of crystalline phases were collected using backscattered electrons with a Quanta 3D field emission scanning electron microscope (Thermo-Fisher Scientific, former FEI) operated at 20 kV and equipped with an EDAX energy-dispersive spectrometer (EDS) Octane Elect Plus. The electron beam current was 4 or 8 nA. The EDS detector was controlled by the TEAM software version 4.6.1. Major components in glass and crystals were analyzed at the GFZ Potsdam using JEOL JXA-8230 Superprobe electron microprobe, and FEI Quanta 3D Dual Beam (SEM&FIB) was used for preliminary study of the run products. The microprobe analyses were performed in WDS mode with an accelerating voltage of 15 kV and beam current of 5, 15, and 20 nA (the best results were obtained with 5 nA). Albite, dolomite, fluorite, and monazite were used as standards for Na, Ca, F, and La. To minimize the damage of carbonate phases by electron beam, we used a defocused beam with a diameter from 20 to 40  $\mu\text{m}$ .

## RESULTS

Run conditions and phase composition of run products are listed in Table 1; typical images of crystalline phases in ground and polished run products are presented in Figure 1, and a summary of electron microprobe analyses of individual phases is given in Tables 2 and 3. Vapor bubbles were observed in all samples, and a separate vapor phase, presumably dominated by  $\text{CO}_2$ , was universally present in addition to crystals and melt, as indicated in Table 1. As discussed below, interpretation of run products was greatly assisted by the unusual ability of La-rich carbonate melts to quench to clear, transparent glass. The low viscosity of carbonatite melts ensured fast crystallization and reaction rates, even at temperatures around 600 °C. Crystal settling was commonly observed in vertically positioned capsules during our experiments.

As mentioned in the introduction, three experiments were carried out on a mixture with the addition of 10 wt%  $\text{Ca}_3(\text{PO}_4)_2$  at 850, 750, and 700 °C (Table 1). Melts in these experiments did not quench to glass but formed fine-grained aggregates of dendritic crystals that are typical quench products of carbonatite and many other salt molten mixtures. Sample BCN-33 was completely crystallized at 700 °C to an aggregate of calcite, nyerereite, apatite, and monazite.

### Crystalline phases

Bastnäsite forms euhedral hexagonal plates up to 100  $\mu\text{m}$  wide and about 10–20  $\mu\text{m}$  thick (Figs. 1a, 1e, and 1f). Its composition is relatively stable and close to the stoichiometric formula, but the measured F content is often lower than the theoretical value of 8.72 wt% (Table 2). The lower F concentrations may be due to analytical errors or  $\text{O}^{2-}$  substituting for 2 F<sup>-</sup>. Bastnäsite contains minor amounts of Ca (0.3–1.3 wt% CaO), which probably substitutes for La in the crystal structure. Sodium is below the detection limit in all the samples.

**TABLE 1.** Run conditions and products

Run no.	Mixture <sup>a</sup>	T, °C	P, MPa	Time, h	Run products <sup>b</sup>
BCN-1	B50:N50	750	100	19	L+V
BCN-2	B50:C50	750	100	19	Bst+Cc+V
BCN-3	B50:N50	700	100	21	L+V
BCN-4	B50:C50	700	100	21	Bst+Cc+V
BCN-5	B20:N80	750	100	72	L+Nc+V
BCN-6	B20:C80	750	100	72	Bst+Cc+trace Fl+V
BCN-7	B50:C30:N20	750	100	72	L+Bst+Bur+V
BCN-8	B50:C50	800	100	20	L+Cc+V
BCN-9	B20:C80	800	100	20	L+Cc+V
BCN-12	B50:N50	650	100	69	L+V
BCN-13	B50:C30:N20	650	100	69	L+Bst+Bur+V
BCN-14	B50:C20:N30	700	100	42	L+Bur+V
BCN-15	B50:C30:N20	725	100	48	L+Bst+Bur+V
BCN-16	B50:C20:N30	650	100	20	L+Bur+minor Bst+V
BCN-18	B50:C20:N30	625	100	64	L+Bur+Luk+V
BCN-19	B50:C30:N20	625	100	64	L+Bst+Bur+Cc+V
BCN-20	B50:C20:N30	750	100	19	L+V
BCN-21	B50:C30:N20	800	100	19	L+V
BCN-22	B50:N50	625	100	23	L+Bur+V
BCN-23	B50:C50	775	100	19	Bst+Cc+trace Fl+V
BCN-24	B20:C60:N20	850	100	48	L+Cc+V
BCN-25	B20:C40:N40	700	100	48	L+Nye+V
BCN-26	B20:C40:N40	650	75	42	L+Nye+V
BCN-27	B20:C60:N20	750	80	42	L+Cc+trace Bst+V
BCN-28	B50:C40:N10	750	100	64	L+Cc+Bst+V
BCN-29	B40:C40:N20	700	100	64	L+Cc+Bur+V
BCN-30	B30:C30:N40	700	100	64	L+V
BCN-34	B30:C30:N40	650	100	600	L+Nye+Burb+V
BCN-35	B40:C40:N20	650	100	26	L+Cc+Burb+V
BCN-37	B50:N50	580	100	48	L+Luk+Nc+V
BCN-38	B30:C20:N50	580	100	48	L+Bur+Nye+Nc+V
BCN-31	B18:C54:N18:C <sub>p</sub> 10	850	100	72	L+Cc+Ap+V
BCN-32	B18:C54:N18:C <sub>p</sub> 10	750	100	48	L+Cc+Ap+V
BCN-33	B18:C54:N18:C <sub>p</sub> 10	700	100	120	Cc+Nye+Ap+Mnz+V

<sup>a</sup> Abbreviations for components: B =  $\text{La}(\text{CO}_3)\text{F}$ ; C =  $\text{CaCO}_3$ ; N =  $\text{Na}_2\text{CO}_3$ ; C<sub>p</sub> =  $\text{Ca}_3(\text{PO}_4)_2$ . Numbers are concentrations of the components in weight percent.

<sup>b</sup> Abbreviations for phases: Ap = apatite, Bst = bastnäsite, Bur = burbankite, Cc = calcite, Fl = fluorite, Luk = lukechangite, Mnz = monazite, Nc = Na carbonate, Nye = nyerereite, L = liquid, V = vapor.

Burbankite in our experiments formed prismatic crystals, which were surrounded in some samples by dendritic overgrowth (Figs. 1a, 1b, 1f, and 1g). In the binary join  $\text{Na}_2\text{CO}_3$ - $\text{La}(\text{CO}_3)\text{F}$  burbankite crystals are surrounded by liquid boundary layers enriched in Na and F where rims of small, micrometer-sized dendritic crystals of Na carbonate formed upon quench (Fig. 1b). Burbankite is a solid solution with a general formula  $\text{A}_3\text{B}_3(\text{CO}_3)_5$ . The A site in natural burbankite is occupied by Na, Ca and may contain vacancies; the B site is filled by larger ions of Sr, Ca, Ba, whereas REE can enter both sites, with preference to the B site (Belovitskaya and Pekov 2004). The composition of burbankite solid solution in our experiments varies broadly from the Ca-free end-member petersenite  $\text{Na}_3(\text{NaLa}_2)(\text{CO}_3)_5$  in the boundary system  $\text{Na}_2\text{CO}_3$ - $\text{La}(\text{CO}_3)\text{F}$  (run BCN-22 in Table 2) to equal molar amounts of Na and Ca and a vacancy in the A site ( $\text{Na}_2\text{Ca}\square)(\text{CaLa}_2)(\text{CO}_3)_5$  in ternary space with the  $\text{CaCO}_3$  component. Mass concentration of  $\text{La}_2\text{O}_3$  in burbankite varies throughout the system from 38 to 46%.

Lukechangite is a fluorocarbonate of Na and La with the ideal formula  $\text{Na}_3\text{La}_2(\text{CO}_3)_4\text{F}$ . It is very rare in nature (Grice and Chao 1997) but abundantly formed in association with burbankite at 625 °C in sample BCN-18 and in association with Na carbonate natrite in run BCN-37 at 580 °C. An alternative Na-La fluorocarbonate arisite (Piilonen et al. 2010) with the formula  $\text{NaLa}_2(\text{CO}_3)_3\text{F}$  clearly does not match the electron microprobe analyses (Table 2). Lukechangite in sample BCN-18 contains

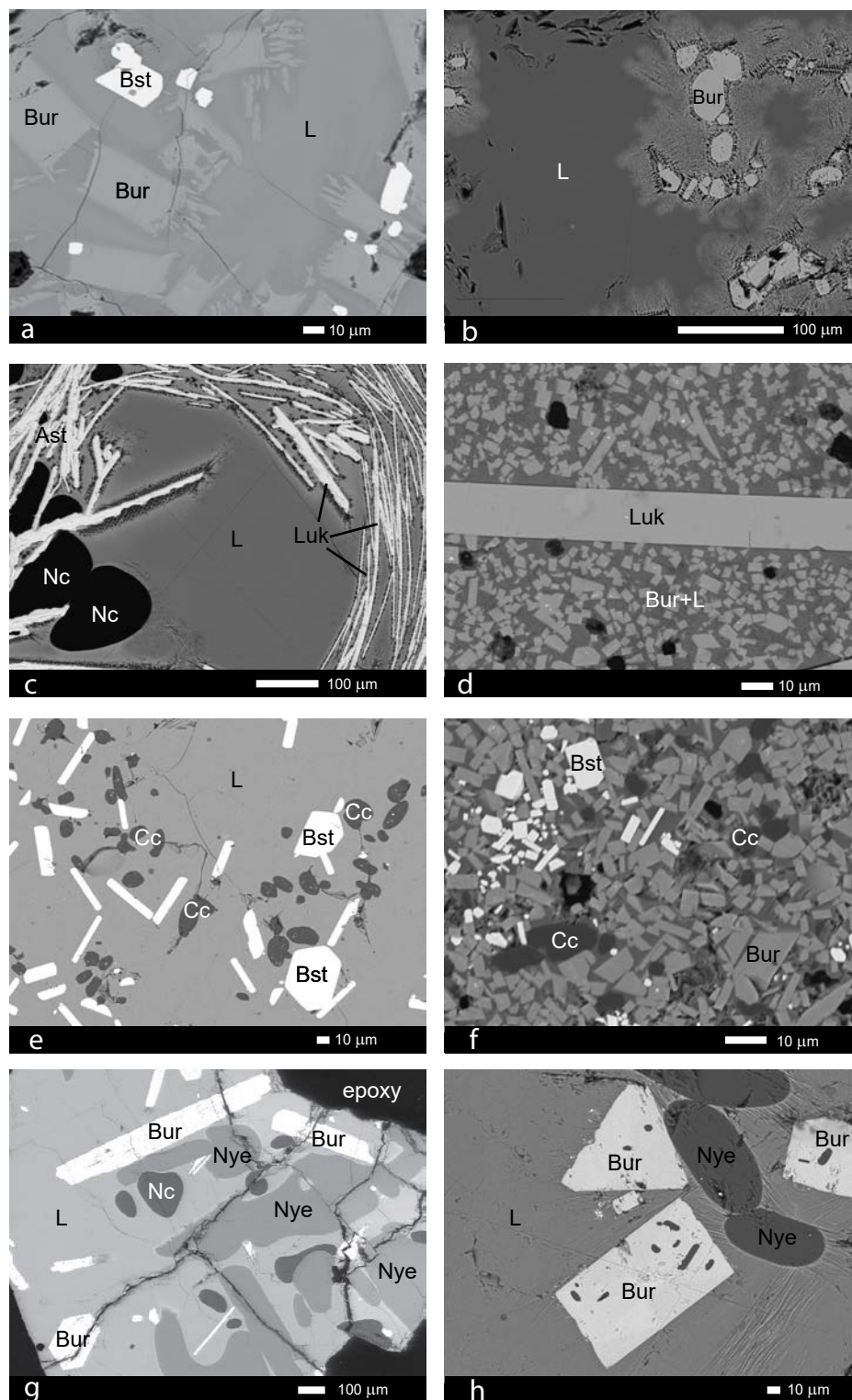


**FIGURE 1.** Backscattered electron images of experimental products. (a) Bastnaesite and burbankite in quenched glass (BCN-7). (b) Prismatic burbankite crystals surrounded by boundary layers enriched in F and dendritic quench natrite (BCN-22). (c) Natrite and lukechangite in sample BCN-37. (d) Burbankite and lukechangite in sample BCN-18. (e) Oval calcite grains and hexagonal plates of bastnaesite in glass (BCN-15). (f) Burbankite, bastnaesite, and minor calcite (BCN-19). (g) Burbankite, nyerereite, and natrite in sample BCN-38; (h) burbankite and nyerereite in sample BCN-34. Abbreviations for phases: Bst = bastnaesite; Bur = burbankite; Cc = calcite; Luk = lukechangite; Nc = natrite; Nye = nyerereite; L = liquid.

**TABLE 2.** Typical compositions of crystal phases in experimental products<sup>a</sup>

Phase	Bastnäsite				Burbankite				Luokechangite	Calcite			Nyerereite	
	Bcn-4	Bcn-7	Bcn-16	Bcn-19	Bcn-18	Bcn-22	Bcn-29	Bcn-34	Bcn-18	Bcn-8	Bcn-15	Bcn-27	Bcn-26	Bcn-34
<i>T</i> , °C	700	750	650	625	625	625	700	650	625	800	700	750	650	650
La <sub>2</sub> O <sub>3</sub> (wt%)	68.32	75.98	68.52	68.06	46.00	44.40	36.33	39.16	50.71	0.19	6.26	2.24	3.82	7.31
CaO	0.87	0.31	0.45	0.59	11.64	0.01	17.14	15.67	1.7	55.47	50.56	53.89	27.93	23.59
Na <sub>2</sub> O	0	0	0.05	0	8.88	16.50	8.88	9.18	13.69	0.01	1.26	0.48	28.81	29.16
F	6.71	5.82	6.63	7.26	0.00	0.00	0.00	0.00	2.3	0.00	0.00	0.00	0.00	0.00
-O=2F	2.82	2.45	2.79	3.06	0.00	0.00	0.00	0.00	0.97	0.00	0.00	0.00	0.00	0.00
Total	73.08	79.67	72.86	72.86	66.52	60.91	62.35	64.02	68.39	55.67	58.1	56.61	59.51	60.05
La (apfu)	0.74	0.95	0.74	0.75	1.85	1.67	1.34	1.49	1.80	0	0.04	0.01	0.05	0.10
Ca	0.03	0.01	0.01	0.02	1.36	0.00	1.84	1.73	0.17	0.99	0.94	0.97	1.05	0.91
Na	0	0	0	0	1.87	3.26	1.72	1.83	2.55	0	0.04	0.02	1.97	2.04
F	0.63	0.62	0.62	0.68	0	0	0	0	0.70	0	0	0	0	0
C <sup>b</sup>	1.08	0.94	1.09	1.1	4.97	5.43	5.14	5.06	4.28	1.01	0.99	1	1.94	1.96
O	3	3	3.00	3	15	15	15	15	12	3	3	3	6	6

<sup>a</sup> Averages of multiple microprobe analyses (number of analyses from 5 to 10).<sup>b</sup> Calculated assuming [CO<sub>2</sub>] = 100 - [Total], in weight percent.**TABLE 3.** Compositions of quenched liquids

Run no.	Mixture	<i>T</i> , °C	<i>n</i>	La <sub>2</sub> O <sub>3</sub> (wt%)		CaO (wt%)		Na <sub>2</sub> O (wt%)		F (wt%)		-O=2F (wt%)	Total
				Avg.	S.D.	Avg.	S.D.	Avg.	S.D.	Avg.	S.D.		
BCN-8	B50:C50	800	6	43.76	0.49	25.49	0.19	0.00	0.00	5.60	0.31	2.36	72.49
BCN-7	B50:C30:N20	750	15	32.48	0.47	16.69	0.16	15.82	0.56	4.52	0.11	1.90	67.60
BCN-15	"	700	20	34.74	0.42	18.14	0.12	13.88	0.38	3.95	0.08	1.66	69.05
BCN-13	"	650	6	34.24	0.26	17.59	0.30	14.23	0.13	5.08	1.10	1.48	68.08
BCN-19	"	625	8	23.40	1.56	19.09	0.44	12.76	0.70	10.28	2.48	4.33	61.20
BCN-14	B50:C20:N30	700	25	35.06	0.33	11.63	0.07	20.20	0.49	3.62	0.11	1.52	68.98
BCN-16	"	650	24	31.69	0.61	12.64	0.13	22.21	0.72	5.10	0.16	2.15	69.50
BCN-18	"	625	21	29.29	0.78	15.14	0.16	21.85	0.75	5.38	0.19	2.27	69.40
BCN-28	B50:C40:N10	750	15	33.88	0.81	18.93	0.25	11.74	0.59	5.06	0.22	2.13	67.48
BCN-29	B40:C40:N20	700	15	29.18	0.65	16.30	0.51	18.43	0.59	4.21	0.29	1.77	66.35
BCN-35	"	650	15	27.07	1.02	17.32	0.69	18.65	1.64	5.05	0.23	2.12	65.96
BCN-34	B30:C30:N40	650	15	20.00	0.61	16.00	0.21	26.31	0.59	2.19	0.10	0.92	63.58
BCN-24	B20:C60:N20	850	20	16.47	0.27	25.38	0.66	21.08	0.85	2.18	0.11	0.92	64.19
BCN-27	"	750	20	19.66	0.50	20.72	0.72	23.01	1.08	2.54	0.18	1.07	64.85
BCN-25	B20:C40:N40	700	20	18.59	0.45	20.45	0.96	25.19	1.00	2.16	0.13	0.91	65.48
BCN-26	"	650	8	13.53	1.60	20.05	2.56	24.24	2.46	2.05	0.81	0.63	58.69
BCN-22	B50:N50	625	5	33.00	0.86	0.00	0.00	28.13	1.55	4.38	0.78	1.84	63.66
BCN-37	"	580	5	28.27	0.61	0.00	0.00	37.04	0.44	3.44	0.76	1.45	63.86
BCN-38	B30:C20:N50	580	7	23.04	0.10	10.67	0.12	37.91	0.91	3.10	0.22	1.31	70.31

Note: Avg. = average and S.D. = standard deviations of *n* microprobe analyses.

1.7 wt% CaO, and in BCN-37 it is Ca-free. Morphologically this phase is very distinct and much different from bastnäsite or burbankite (Figs. 1c and 1d). It forms thin hexagonal plates measuring up to 500 μm in width and only 20–30 μm in thickness.

Calcite forms rounded oval crystals (Figs. 1e and 1f) with an average size broadly variable from run to run depending on the nucleation density. In the binary system CaCO<sub>3</sub>-La(CO<sub>3</sub>)F, calcite contains <1 wt% La<sub>2</sub>O<sub>3</sub>, and it is close to the theoretical formula. In contrast, calcite crystallizing from ternary mixtures contains up to 8 wt% La<sub>2</sub>O<sub>3</sub> and up to 1.8 wt% Na<sub>2</sub>O. Calcite crystals in runs BCN-27 and -29 are strongly zoned from La-poor cores to La-rich rims. Linear correlation between La and Na concentrations corresponds to equimolar substitution of La<sup>3+</sup> and Na<sup>+</sup> for 2 Ca<sup>2+</sup> in calcite crystal structure. Therefore, the calcite-melt distribution coefficient (*D*) for La primarily depends on Na/Ca ratio of the melt, and it tends to decrease with falling temperature. It is only 0.004 in the Na-free run BCN-8; 0.4 in run BCN-24; and 0.1 in run BCN-27. Notably, the formation of REE-rich calcite was also observed by Mollé et al. (2021) in experiments involving complex Na-bearing carbonatite compositions.

Nyerereite is observed as large (up to 200 × 300 μm) sub-hedral prisms and rounded, anhedral aggregates (Figs. 1g and 1h). It contains up to 7.3 wt% La<sub>2</sub>O<sub>3</sub> (Table 2) and Na, slightly in excess of the ideal formula Na<sub>2</sub>Ca(CO<sub>3</sub>)<sub>2</sub>. It appears that in

this system, nyerereite, like calcite, shows significant isomorphic substitution 2 Ca<sup>2+</sup> → La<sup>3+</sup> + Na<sup>+</sup>. The nyerereite/melt distribution coefficient for La varies in samples BCN-26 and BCN-34 between 0.28 and 0.37. Notably, natural nyerereite phenocrysts in natrocarbonatite lava also show high concentrations of REE (Zaitsev et al. 2009), and distribution coefficients comparable with those in our experiments.

Sodium carbonate (presumably natrite) formed rounded, irregular drop-like and oval grains with an average size of about 150 μm (Figs. 1c and 1g). Run products containing this phase were very fragile, hygroscopic and unstable during grinding and polishing, but we managed to prepare epoxy mounts of samples BCN-37 and BCN-38 suitable for microprobe analyses. According to the analyses, natrite in the Ca-free sample BCN-37 contains a few weight percent La<sub>2</sub>O<sub>3</sub>, and in sample BCN-38 it contains up to 10 wt% CaO and 3.2 wt% La<sub>2</sub>O<sub>3</sub>.

A few grains of fluorite were found in subsolidus of the CaCO<sub>3</sub>-La(CO<sub>3</sub>)F binary system in association with bastnäsite and calcite. According to electron microprobe analyses, fluorite composition is close to pure CaF<sub>2</sub> with only small amounts of La (around 0.2 wt% La<sub>2</sub>O<sub>3</sub>).

Fluorapatite in samples BCN-31 and BCN-32 formed numerous small rounded grains that are often too small for electron microprobe analyses. Fluorapatite crystals in BCN-33 are bigger,

many of them are euhedral and up to 15–20  $\mu\text{m}$  in size. The phase contains on average 2.1 wt%  $\text{Na}_2\text{O}$  and 4.7 wt%  $\text{La}_2\text{O}_3$ . This implies isomorphic substitution  $2\text{Ca}^{2+} \rightarrow \text{La}^{3+} + \text{Na}^+$  that is characteristic of the natural phosphate mineral belovite-(La) belonging to the apatite supergroup (Kabalova et al. 1997).

Monazite in sample BCN-33 is observed as small euhedral prismatic crystals up to 10  $\mu\text{m}$  in length. Its composition is close to the ideal formula  $\text{LaPO}_4$ .

### Liquid phase and La solubility

Jones and Wyllie (1983) were probably the first who discovered that carbonate melts with high-La content, in contrast to the vast majority of carbonatite liquids, quenched to homogenous glass at normal quenching rates used in experimental petrology. In our experiments, melts were quenched to clear transparent glass in all the binary and ternary starting mixtures with 30–50 wt% of the  $\text{La}(\text{CO}_3)\text{F}$  component. Melts with  $\text{La}_2\text{O}_3$  contents below 20 wt% quenched to fine-grained dendritic crystals of calcite and Na- and La-rich carbonate matrix that is typical for quenched carbonatite liquids (e.g., Fig. 1h).

The solubility of La in liquids saturated in bastnäsité and burbankite solid solution produced in our experiments depends on the temperature and Na/Ca ratio of the melt composition. Notably, the two variables are interdependent as melt saturation in La minerals tends to be reached at a lower temperature in compositions with high Na/Ca. Compositions most relevant for natural carbonatite magma are those that are saturated with both calcite and bastnäsité. A few samples meeting this requirement (Table 3) range from Na-free BCN-8 at 800 °C, where  $\text{La}_2\text{O}_3$  concentration in liquid is at 43.8 wt% to BCN-27 at 750 °C with  $\text{La}_2\text{O}_3$  in the liquid at 19.7 wt% and the molar Na/Ca ratio of 2. Thus, La solubility in liquids saturated in calcite and bastnäsité tends to decrease with falling temperature and increasing Na/Ca in the liquid down to about 20 wt%. Liquid saturated in burbankite and nyerereite at 650 °C also contains 20 wt%  $\text{La}_2\text{O}_3$  (sample BCN-34 in Table 3), so this solubility of La appears to be minimal for all the studied compositions. Notably, total REE concentration in the bastnäsité-saturated, multicomponent carbonatitic melt that modeled natural compositions in the experiments by Mollé et al. (2021) at 600 °C and 100 MPa was also at the concentration level of ~20 wt%  $\text{La}_2\text{O}_3$ .

Liquid compositions in phosphate-bearing samples BCN-31 and BCN-32 were not analyzed because of strong interference with small apatite crystals and the lack of crystal-free areas suitable for reliable microprobe analyses.

### Phase equilibria in the system $\text{La}(\text{CO}_3)\text{F}-\text{CaCO}_3-\text{Na}_2\text{CO}_3$

**Solidus assemblages.** As described in the previous section, burbankite, nyerereite, and calcite in  $\text{La}(\text{CO}_3)\text{F}-\text{CaCO}_3-\text{Na}_2\text{CO}_3$  ternary mixtures form solid solutions that contain significant amounts of La but no detectable F. This and the presence of  $\text{CO}_2$ -dominated vapor implies that the system  $\text{La}(\text{CO}_3)\text{F}-\text{CaCO}_3-\text{Na}_2\text{CO}_3$  at the conditions of our experiments is, in fact, a pseudoternary join of a five-component system where NaF and  $\text{CO}_2$  are independent components. In Figure 2 we use trigonal-prismatic composition space for plotting the positions of all the mineral phases encountered in the studied part of the quinary system  $\text{La}^{3+}-\text{Ca}^{2+}-\text{Na}^+-\text{CO}_3^{2-}-\text{F}^-$  and have connected equilibrium

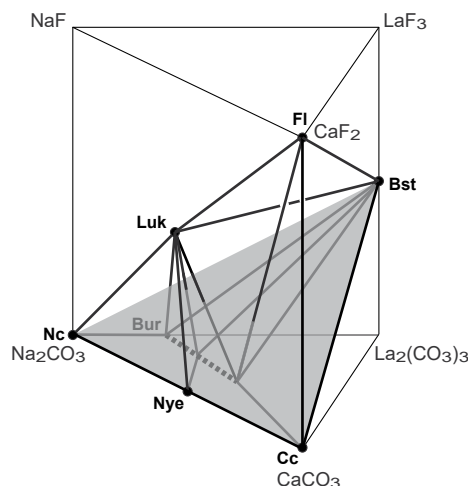


**FIGURE 2.** The positions of equilibrium crystalline phases and stable solidus assemblages plotted in the trigonal-prismatic compositional space  $\text{CaCO}_3-\text{Na}_2\text{CO}_3-\text{La}_2(\text{CO}_3)_3-\text{CaF}_2-\text{NaF}-\text{LaF}_3$ . The studied pseudoternary join  $\text{CaCO}_3-\text{Na}_2\text{CO}_3-\text{La}(\text{CO}_3)\text{F}_2$  is shown as semi-transparent gray triangle. Phase compositions are plotted in molar units. The extent of burbankite solid solutions is shown by dotted line. Abbreviations for phases: Bst = bastnäsité; Bur = burbankite; Cc = calcite; Luk = lukechangite; Fl = fluorite; Nc = natrite; Nye = nyerereite.

mineral assemblages with the Alkemade lines. For simplicity, minor compositional variations of calcite and nyerereite solid solutions are ignored, and only burbankite is shown as a phase of variable composition.

According to the phase rule, the maximal number of crystalline phases that can be equilibrated with liquid and vapor in an isobaric quinary system is 4. The topology of phase equilibria shown in Figure 2 implies that the solidus mineral assemblages within the studied pseudoternary join are: bastnäsité-burbankite-fluorite-calcite, bastnäsité-burbankite-fluorite-lukechangite, bastnäsité-burbankite-lukechangite, burbankite-lukechangite-nyerereite-calcite, and burbankite-lukechangite-nyerereite-natrite.

**Liquidus equilibria.** Triangular phase diagram in Figure 3 presents a projection of liquidus phase equilibria in the studied part of the pseudoternary system. Information on melting in the binary boundary join  $\text{Na}_2\text{CO}_3-\text{CaCO}_3$  at 100 MPa is taken from Cooper et al. (1975). Pure  $\text{Na}_2\text{Ca}(\text{CO}_3)_2$  end-member nyerereite that melts congruently at 817 °C is an intermediate compound in the binary. Another intermediate compound, shortite  $\text{Na}_2\text{Ca}_2(\text{CO}_3)_3$ , is stable only in subsolidus below 400 °C and is not shown in Figure 3. The extent of solid solutions (thick gray lines) is based on the electron microprobe data (Table 2). The compositions of burbankite *a* and *b* that coexist with calcite, nyerereite, and lukechangite were determined by electron microprobe in samples BCN-29, BCN-34, and BCN-18 (Table 2). Unlike the diagram in Figure 2 that is scaled in molar units, the pseudoternary join in Figure 3 is drawn in weight percent. One should also bear in mind that the solid solutions and some of the key Alkemade lines shown in Figure 3 lie off the plane of the join (see Fig. 2) and are projected onto it. The projection is done by recalculating mass concentrations of  $\text{Na}_2\text{O}$ , CaO, and

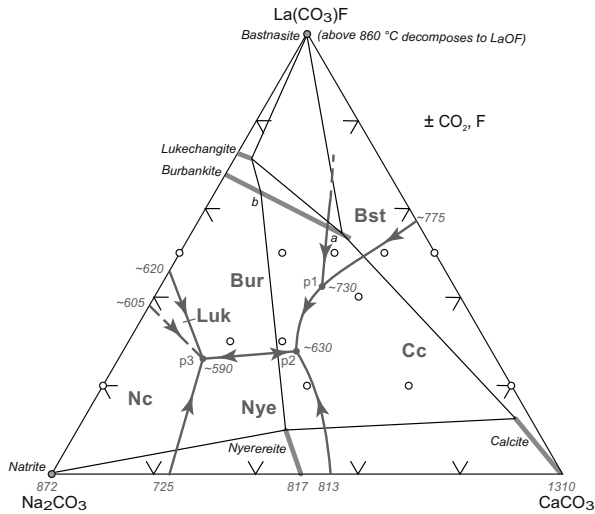
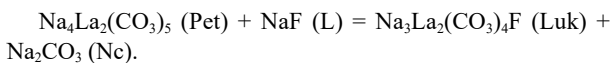


**FIGURE 3.** Pseudoternary phase diagram of the system  $\text{CaCO}_3$ - $\text{Na}_2\text{CO}_3$ - $\text{La}(\text{CO}_3)_2\text{F}_2$  at 100 MPa in weight percent. The positions of starting mixtures are plotted as open circles. Primary crystallization fields on liquidus surface are outlined and labeled in arrowed gray lines. Numbers are temperature estimations in degrees Celsius. See text for discussion.

$\text{La}_2\text{O}_3$  determined for a given phase by electron microprobe to the normative components  $\text{Na}_2\text{CO}_3$ ,  $\text{CaCO}_3$ , and  $\text{La}(\text{CO}_3)_2\text{F}_2$  and normalizing the latter to 100%.

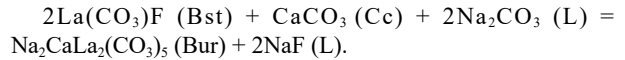
Mineral stability fields on the liquidus surface that were observed in the temperature interval between 580 and 850 °C are outlined and labeled in Figure 3 in red. The concentration of  $\text{La}(\text{CO}_3)_2\text{F}_2$  component in our starting mixtures did not exceed 50 wt%, and the most La-rich part of the join has not been studied. However, previous studies imply that the part of the liquidus surface not covered by our experiments should be dominated by the stability field of  $\text{LaOF}$  that should replace bastnaesite above 860 °C (Hsu 1992).

If a few fluorite crystals in subsolidus samples BCN-6 and BCN-23 are ignored [fluorite probably appeared because of a minor excess of  $\text{LaF}_3$  over  $\text{La}_2(\text{CO}_3)_3$  in the starting mixtures], liquidus relationships between calcite and bastnaesite in the boundary join  $\text{CaCO}_3$ - $\text{La}(\text{CO}_3)_2\text{F}_2$  can be interpreted as a binary eutectic at 775 ± 20 °C and 58 wt% of the  $\text{La}(\text{CO}_3)_2\text{F}_2$  component. Other minerals of the bastnaesite group (synchisite, parasite, and röntgenite) did not form and are probably subsolidus phases. Phase relationships in the boundary join  $\text{Na}_2\text{CO}_3$ - $\text{La}(\text{CO}_3)_2\text{F}_2$  are, however, more complex. Lukechangite (Luk), natrite (Nc), and Ca-free end-member of burbankite solid solution petersenite (Pet) are involved in a peritectic reaction with liquid (L):



The right-hand side assemblage becomes stable between 580 and 625 °C (samples BCN-22 and BCN-37). The peritectic relationships between burbankite solid solution and lukechangite apparently extend to Ca-bearing ternary compositions.

Another peritectic reaction in the quinary composition space involves bastnaesite (Bst), calcite (Cc), and burbankite (Bur):



The equation implies that the assemblage Bst+Cc becomes unstable at a certain critical concentration of Na carbonate component in liquid, and bastnaesite is replaced by burbankite solid solution. The replacement of bastnaesite by burbankite in calcite-saturated compositions takes place approximately below 730 °C (see point p1 in Fig. 3). Crystallization of burbankite, in turn, leads to the accumulation of NaF component in melt. At advanced stages of crystallization and according to the first peritectic reaction, NaF component of the liquid and some burbankite react back and form lukechangite, e.g., in solidus assemblages with nyerereite and natrite. As shown in Figure 2, burbankite and lukechangite lie on the opposite sides of the studied pseudoternary join, and their liquidus relationships are difficult to plot in the projection. Nevertheless, liquid compositions in samples BCN-34 and BCN-38 (Table 3) give approximate positions of the “piercing points” p2 and p3. Liquid of the composition p2 should crystallize to solidus assemblage Bur+Nye+Cc+Luk, whereas on further cooling liquid p3 should produce solidus assemblage Bur+Nye+Nc+Luk.

#### The effects of phosphate component

Starting mixture B18:C54:N18:CP10 (Table 1) initially contains 13.46 wt%  $\text{La}_2\text{O}_3$ , 4.58 wt%  $\text{P}_2\text{O}_5$ , and has the molar La/P = 1.28. Despite the significant molar excess of La over P and extensive crystallization of apatite removing  $\text{P}_2\text{O}_5$  together with CaO from the melt, La carbonates and fluorocarbonates are totally absent from the solidus assemblage where La is distributed between monazite and apatite, calcite and nyerereite solid solutions. As noted above, solidus apatite contains 4.7 wt%  $\text{La}_2\text{O}_3$ , and the  $\text{La}_2\text{O}_3$  concentrations in calcite and nyerereite are 0.89 and 7.14 wt%, respectively. Our results confirm that REE phosphate minerals are much more stable during magmatic crystallization than REE (fluoro)carbonate species and at typical concentrations of REE and P in carbonatite magma, apatite and monazite should be the only primary magmatic hosts of REE.

#### DISCUSSION

This study is, to the best of our knowledge, the first experimental demonstration that bastnaesite and burbankite can co-crystallize from carbonatite melt at *P-T* conditions relevant for crustal carbonatite magmas. Our experiments show that fluorobastnaesite crystallizes together with burbankite and calcite from melts with low to moderate Na contents, whereas burbankite and lukechangite completely replace bastnaesite in bulk compositions with Na/Ca molar ratio above 2. The demonstration that bastnaesite and burbankite can readily crystallize from carbonate melt in laboratory experiments on synthetic mixtures does not, however, prove the magmatic origin of minerals in nature. Our experiments revealed two major obstacles for magmatic crystallization of REE (fluoro)carbonates. The first is the very high solubility of REE at about 15–20 wt%, which was also observed in previous studies (Jones and Wyllie 1983, 1986; Wyllie et al. 1996). Such REE concentrations are hardly attainable in natural carbonatite magmas. The second is the much greater stability of REE phosphate minerals at magmatic conditions in comparison

with (fluoro)carbonates and the high capacity of calcite and apatite for incorporating REE in their crystal structures. It should be noted, though, that carbonatites at Mountain Pass are possibly a unique exception in this respect. They are characterized by very low  $P_2O_5$  concentrations, mostly below 0.5 wt% (Castor 2008), and extreme enrichment in REE at a level that could have allowed bastnäsite to out-compete REE-bearing phosphate minerals. However, the origin of such unusual carbonatite magma is controversial. If Mountain Pass bastnäsite deposit is indeed magmatic, its origin is possibly rooted in an exceptionally enriched mantle source (Poletti et al. 2016).

Carbonatite derivatives of nephelinitic-melilititic magmas that are most common have high-P/REE values that make primary magmatic crystallization of bastnäsite and burbankite very unlikely, if not impossible. Natrocarbonatite lava, in this regard, is an extreme and probably the best-studied example of derivative carbonatite produced from nephelinitic magma by a combination of fractional crystallization and silicate-carbonate liquid immiscibility. The concentrations of  $P_2O_5$  and REE in natrocarbonatite are at about 0.75 wt% and 1800 ppm, respectively (Keller and Spettel 1995), and thus the molar REE/P is at about 0.12. This is ten times lower than the La/P molar ratio in our phosphate-bearing mixture, where bastnäsite and burbankite were completely replaced by apatite and monazite.

However, as mentioned in the introduction, burbankite and bastnäsite are ubiquitous in typical intrusive carbonatites. In some cases, burbankite has been observed to form large (centimeter-sized), euhedral crystals that look like products of primary crystallization (Chakhmouradian and Zaitsev 2012). Therefore, there must be some way for REE in intrusive carbonatites to bypass phosphate precipitation and form carbonate minerals.

Traces of a possible parental media for precipitation of REE carbonates have probably been found in fluid inclusions associated with plutonic carbonatites. Numerous studies (e.g., Bühn and Rankin 1999; Bühn et al. 2002; Rankin 2005; Walter et al. 2020) have reported inclusions in minerals from carbonatites, and their exocontact zones that contained highly concentrated chloride-carbonate-sulfate brines with up to 3.7 wt% REE, 0.6–3 wt% F and no detectable phosphate. The brines are strongly enriched in alkalis and have been interpreted as fluids responsible for fenitization that is universally observed at contacts with intrusive carbonatites. If such fluids so enriched in REE are not expelled from carbonatite, they should be capable of forming REE mineralization within carbonatite body. In good agreement with our experiments, burbankite (not bastnäsite) was found among the daughter minerals of the brine inclusions in association with Na bicarbonate nahcolite (Bühn and Rankin 1999; Bühn et al. 2002). The content of  $H_2O$  in the fluid has been estimated at about 20 wt%, and some researchers prefer to call it a salt melt (Rankin 2005). Such fluids or melts seem to be routinely produced by common intrusive carbonatites, possibly at the magmatic-hydrothermal transition.

Evidence is growing for an important role of hydrothermal fluids in the origin of the world's largest bastnäsite deposit at Bayan Obo in China (Yang et al. 2017 and references therein). Primary fluid inclusions are poorly preserved in Bayan Obo minerals, but Fan et al. (2004, 2006) reported REE daughter minerals (presumably bastnäsite and ceibaite) in inclusions of alkaline

carbonate-chloride brines. Smith et al. (1999) described reaction textures in aegirine-magnetite-fluorite rocks and hydrothermally altered dolomite marble where monazite in immediate contact with calcite or dolomite had been replaced by a fine-grained aggregate of bastnäsite and apatite. These observations imply that in hydrothermal systems at favorable conditions (high activities of F and carbonate ions and elevated pH), bastnäsite can become more stable than monazite.

## IMPLICATIONS

Despite liquidus crystallization of bastnäsite and burbankite in synthetic model system  $La(CO_3)F-CaCO_3-Na_2CO_3$ , primary magmatic crystallization of REE carbonates and fluorocarbonates from natural carbonatitic melts is unlikely (with a possible exception of the uniquely REE-rich and  $P_2O_5$ -poor carbonatites at Mountain Pass). The reason lies in the much greater stability of REE-bearing phosphate minerals such as apatite and monazite under magmatic conditions. Carbonate and fluorocarbonate REE minerals in carbonatites are likely to crystallize from highly concentrated brines that are mostly composed of alkali carbonates, chlorides, sulfates, and fluorides. Traces of such brines have been found in fluid inclusions, and the fluids are believed to be responsible for the widespread fenitization of country rocks around carbonatite bodies. Studies of fluid inclusions demonstrated that the brines are capable of dissolving large amounts of REE (e.g., Bühn and Rankin 1999; Rankin 2005). The example of giant bastnäsite deposits at Bayan Obo in China shows that protracted fluid activity and multiple episodes of REE mobilization and redeposition may be required for bastnäsite accumulation at an economic level. A large body of thermodynamic and experimental data is available for chloride, fluoride, and sulfate complexes of REE at hydrothermal conditions, but the information is sparse for carbonate complexes (Migdisov et al. 2016 and references therein). It is also not clear to what extent data on relatively dilute solutions is applicable to brines with characteristics approaching those of hydrated melts. Therefore, mechanisms behind the formation of alkaline carbonate-chloride brines in carbonatite systems, their properties, and their role in the transport and concentration of REE and other critical metals appear to be important and promising subjects for future research.

## ACKNOWLEDGMENTS AND FUNDING

We thank Oona Appelt for help with EMP analyses of experimental products. Thoughtful and constructive reviews by Bruce Kjarsgaard, David Dolejš, and an anonymous colleague inspired us to do additional experiments and improve the original version of the paper. The project was supported by RSF Grant No. 19-17-00013.

## REFERENCES CITED

- Belovitskaya, Y.V., and Pekov, I.V. (2004) Genetic mineralogy of the burbankite group. *New Data on Minerals*, 39, 50–64.
- Brooker, R., Holloway, J.R., and Hervig, R. (1998) Reduction in piston-cylinder experiments: The detection of carbon infiltration into platinum capsules. *American Mineralogist*, 83, 985–994.
- Bühn, B., and Rankin, A.H. (1999) Composition of natural, volatile-rich Na-Ca-REE-Sr carbonatitic fluids trapped in fluid inclusions. *Geochimica et Cosmochimica Acta*, 63, 3781–3797.
- Bühn, B., Rankin, A.H., Schneider, J., and Dulski, P. (2002) The nature of orthomagmatic, carbonatitic fluids precipitating REE, Sr-rich fluorite: Fluid inclusions evidence from the Okorusu fluorite deposit. *Chemical Geology*, 186, 75–98.
- Castor, S.B. (2008) The Mountain Pass rare-earth carbonatite and associated ultrapotassic rocks, California. *Canadian Mineralogist*, 46, 779–806.
- Chakhmouradian, A.R., and Zaitsev, A.N. (2012) Rare earth mineralization in igneous

- rocks: Sources and processes. *Elements*, 8, 347–353.
- Cooper, A.F., Gittins, J., and Tuttle, O.F. (1975) The system  $\text{Na}_2\text{CO}_3\text{-K}_2\text{CO}_3\text{-CaCO}_3$  at 1 kbar and its significance in carbonatite petrogenesis. *American Journal of Science*, 275, 534–560.
- Donnay, G., and Donnay, J.D.H. (1953) The crystallography of bastnäsite, parisite, roentgenite, and synchisite. *American Mineralogist*, 38, 932–963.
- Fan, H.R., Xie, Y.H., Wang, K.Y., Tao, K.J., and Wilde, S.A. (2004) REE daughter minerals trapped in fluid inclusions in the giant Bayan Obo REE-Nb-Fe deposit, Inner Mongolia, China. *International Geology Review*, 46, 638–645.
- Fan, H.R., Hu, F.F., Yang, K.F., and Wang, K.Y. (2006) Fluid unmixing/immiscibility as an ore-forming process in the giant REE-Nb-Fe deposit, Inner Mongolian, China: evidence from fluid inclusions. *Journal of Geochemical Exploration*, 89, 104–107.
- Fleischer, M. (1978) Relative proportions of the lanthanides in minerals of the bastnäsite group. *Canadian Mineralogist*, 16, 361–363.
- Gittins, J., and Jago, B.C. (1998) Differentiation of natrocarbonatite magma at Oldoinyo Lengai volcano, Tanzania. *Mineralogical Magazine*, 62, 759–768.
- Grice, J.D., and Chao, G.Y. (1997) Lukechangite-(Ce), a new rare-earth-fluorocarbonate mineral from Mont Saint-Hilaire, Quebec. *American Mineralogist*, 82, 1255–1260.
- Guzmics, T., Zajacz, Z., Mitchell, R.H., Szabó, C., and Wälle, M. (2015) The role of liquid-liquid immiscibility and crystal fractionation in the genesis of carbonatite magmas: insights from Kerimasi melt inclusions. *Contributions to Mineralogy and Petrology*, 169, 17.
- Haschke, J.M. (1975) The lanthanum hydroxide fluoride carbonate system: The preparation of synthetic bastnäsite. *Journal of Solid State Chemistry*, 12, 115–121.
- Hsu, L.C. (1992) Synthesis and stability of bastnäsites in a part of the system (Ce,Ln)-F-H-C-O. *Mineralogy and Petrology*, 47, 87–101.
- Janka, O., and Schleid, T. (2009) Facile synthesis of bastnäsite-type  $\text{LaF}[\text{CO}_3]$  and its thermal decomposition to LaOF for bulk and  $\text{Eu}^{3+}$ -doped samples. *European Journal of Inorganic Chemistry*, 2009, 357–362.
- Jansen, G.J., Magin, G.B., and Levin, B. (1959) Synthesis of bastnäsite. *American Mineralogist*, 44, 180–181.
- Jones, A., and Wyllie, P. (1983) Low-temperature glass quenched from a synthetic, rare earth carbonatite: implications for the origin of the Mountain Pass deposit. *Economic Geology*, 78, 1721–1723.
- (1986) Solubility of rare earth elements in carbonatite magmas, indicated by the liquidus surface in  $\text{CaCO}_3\text{-Ca}(\text{OH})_2\text{-La}(\text{OH})_3$  at 1 kbar pressure. *Applied Geochemistry*, 1, 95–102.
- Kabalova, Y.K., Sokolova, E.V., and Pekov, I.V. (1997) Crystal structure of belovite-(La). *Doklady Akademii Nauk*, 355, 182–185.
- Keller, J., and Spettel, B. (1995) The trace element composition and petrogenesis of natrocarbonatites. In K. Bell and J. Keller, Eds. *Carbonatite Volcanism*, p. 70–86. Springer.
- Kjarsgaard, B.A. (1998) Phase relations of a carbonated high-CaO nephelinite at 0.2 and 0.5 GPa. *Journal of Petrology*, 39, 2061–2075.
- Kjarsgaard, B.A., Hamilton, D.L., and Peterson, T.D. (1995) Peralkaline nephelinite/carbonatite liquid immiscibility: comparison of phase compositions in experiments and natural lavas from Oldoinyo Lengai. In K. Bell and J. Keller, Eds., *Carbonatite Volcanism*, p. 163–190. Springer.
- Lee, M.H., and Jung, W.S. (2013) Hydrothermal synthesis of  $\text{LaCO}_3\text{OH}$  and  $\text{Ln}^{3+}$ -doped  $\text{LaCO}_3\text{OH}$  powders under ambient pressure and their transformation to  $\text{La}_2\text{O}_3\text{CO}_3$  and  $\text{La}_2\text{O}_3$ . *Bulletin of the Korean Chemical Society*, 34, 3609–3614.
- Lee, W.-J., and Wyllie, P.J. (1998) Processes of crustal carbonatite formation by liquid immiscibility and differentiation, elucidated by model systems. *Journal of Petrology*, 39, 2005–2013.
- Mathews, W., Linnen, R.L., and Guo, Q. (2003) A filler-rod technique for controlling redox conditions in cold-seal pressure vessels. *American Mineralogist*, 88, 701–707.
- Mercier, N., Taulelle, F., and Leblanc, M. (1993) Growth, structure, NMR characterization of a new fluorocarbonate  $\text{Na}_3\text{La}_2(\text{CO}_3)_4\text{F}$ . *European Journal of Solid State and Inorganic Chemistry*, 30, 609–617.
- Migdisov, A., Williams-Jones, A.E., Brugger, J., and Caporuscio, F.A. (2016) Hydrothermal transport, deposition, and fractionation of the REE: Experimental data and thermodynamic calculations. *Chemical Geology*, 439, 13–42.
- Mollé, V., Gaillard, F., Naby, Z., Tuduri, J., Iacono-Marziano, G., Di Carlo, I., and Erdmann, S. (2021) Experimental crystallisation of a REE-rich calcio-carbonatitic melt: crystallisation sequence and REE behaviour. *EMPG-XVII Conference Abstracts*, 61.
- Montes-Hernandez, G., Chiriac, R., Findling, N., Toche, F., and Renard, F. (2016) Synthesis of ceria ( $\text{CeO}_2$  and  $\text{CeO}_2\text{-x}$ ) nanoparticles via decarbonation and Ce(III) oxidation of synthetic bastnäsite ( $\text{CeCO}_3\text{F}$ ). *Materials Chemistry and Physics*, 172, 202–210.
- Naby, Z., Massuyeau, M., Gaillard, F., Tuduri, J., Iacono-Marziano, G., Rogerie, G., Le Trong, E., Di Carlo, I., Melleton, J., and Bailly, L. (2020) A window in the course of alkaline magma differentiation conducive to immiscible REE-rich carbonatites. *Geochimica et Cosmochimica Acta*, 282, 297–323.
- Nielsen, T.F.D., Solovova, I.P., and Veksler, I.V. (1997) Parental melts of melilitolite and origin of alkaline carbonatite: evidence from crystallised melt inclusions, Gardiner complex. *Contributions to Mineralogy and Petrology*, 126, 331–344.
- Panina, L.I. (2005) Multiphase carbonate-salt immiscibility in carbonatite melts: data on melt inclusions from the Krestovskiy massif minerals (Polar Siberia). *Contributions to Mineralogy and Petrology*, 150, 19–36.
- Pilonen, P.C., McDonald, A.M., Grice, J.D., Cooper, M.A., Kolitsch, U., Rowe, R., Gault, R.A., and Poirier, G. (2010) Arisite-(La), a new REE-fluorocarbonate mineral from the Aris phonolite (Namibia), with descriptions of the crystal structures of arisite-(La) and arisite-(Ce). *Mineralogical Magazine*, 74, 257–268.
- Poletti, J.E., Cottle, J.M., Hagen-Peter, G.A., and Lackey, J.S. (2016) Petrochronological constraints on the origin of the Mountain Pass ultrapotassic and carbonatite intrusive suite, California. *Journal of Petrology*, 57, 1555–1598.
- Pradip, and Fuerstenau, D.W. (2013) Design and development of novel flotation reagents for the beneficiation of Mountain Pass rare-earth ore. *Mining, Metallurgy & Exploration*, 30, 1–9. <https://doi.org/10.1007/BF03402335>
- Rankin, A.H. (2005) Carbonate-associated rare metal deposits: composition and evolution of ore-forming fluids—The fluid inclusions evidence. In R.L. Linnen and I.M. Samson, Eds., *Rare-Element Geochemistry and Ore Deposits*. *GAC Short Course Notes*, 17, p. 299–314.
- Rowland, R.L. II (2017) Phase equilibria, compressibility, and thermal analysis of bastnaesite-(La). Ph.D. thesis, University of Nevada.
- Rowland, R.L. II, Lavina, B., Kaaden, K.E.V., Danielson, L.R., and Burnley, P.C. (2020) Thermal analysis, compressibility, and decomposition of synthetic bastnäsite-(La) to lanthanum oxyfluoride. *Minerals*, 10, 212
- Shivaramaiah, R., Anderko, A., Riman, R.E., and Navrotsky, A. (2016) Thermodynamics of bastnäsite: A major rare earth ore mineral. *American Mineralogist*, 101, 1129–1134.
- Smith, M.P., Henderson, P., and Peishan, Z. (1999) Reaction relationships in the Bayan Obo Fe-REE-Nb deposit Inner Mongolia, China: implications for the relative stability of rare-earth element phosphates and fluorocarbonates. *Contributions to Mineralogy and Petrology*, 134, 294–310.
- Sokolov, S.V., Veksler, I.V., and Senin, V.G. (1999) Alkalis in carbonatite magmas: new evidence from melt inclusions. *Petrology*, 7, 602–609.
- Veksler, I.V., and Keppler, H. (2000) Partitioning of Mg, Ca, and Na between carbonatite melt and hydrous fluid at 0.1–0.2 GPa. *Contributions to Mineralogy and Petrology*, 138, 27–34.
- Veksler, I.V., Nielsen, T.F.D., and Sokolov, S.V. (1998) Mineralogy of crystallized melt inclusions from Gardiner and Kovdor ultramafic alkaline complexes: implications for carbonatite genesis. *Journal of Petrology*, 39, 2015–2031.
- Von Eckeremann, H. (1966) Progress of research on the Alnö carbonatite. In O.F. Tuttle and J. Gittins, Eds., *Carbonatites*, p. 3–31. Wiley.
- Walter, B.F., Steele-MacInnis, M., Giebel, R.J., Marks, M.A., and Markl, G. (2020) Complex carbonate-sulfate brines in fluid inclusions from carbonatites: Estimating compositions in the system  $\text{H}_2\text{O-Na-K-CO}_3\text{-SO}_4\text{-Cl}$ . *Geochimica et Cosmochimica Acta*, 277, 224–242.
- Weidendorfer, D., Schmidt, M.W., and Mattsson, H.B. (2017) A common origin of carbonatite magmas. *Geology*, 45, 507–510.
- Williams-Jones, A.E., and Wood, S.A. (1992) A preliminary petrogenetic grid for REE fluorocarbonates and associated minerals. *Geochimica et Cosmochimica Acta*, 56, 725–738.
- Wyllie, P.J., and Tuttle, O.F. (1960) The system  $\text{CaO-CO}_2\text{-H}_2\text{O}$  and the origin of carbonatites. *Journal of Petrology*, 1, 1–46.
- Wyllie, P.J., Jones, A.P., and Deng, J. (1996) Rare earth elements in carbonate-rich melts from mantle to crust. In A.P. Jones, F. Wall, and C.T. Williams, Eds. *Rare Earth Minerals: Chemistry, Origin and Ore Deposits*. *Mineralogical Society U.K. Special Publications*, 7, p. 77–103. Chapman & Hall.
- Yang, X., Lai, X., Pirajno, F., Liu, Y., Mingxing, L., and Sun, W. (2017) Genesis of the Bayan Obo Fe-REE-Nb formation in Inner Mongolia, north China craton: a perspective review. *Precambrian Research*, 288, 39–71.
- Zaitsev, A.N., Demény, A., Sindern, S., and Wall, F. (2002) Burbankite group minerals and their alteration in rare earth carbonatites—source of elements and fluids (evidence from C-O and Sr-Nd isotopic data). *Lithos*, 62, 15–33.
- Zaitsev, A.N., Keller, J., Spratt, J., Jeffries, T.E., and Sharygin, V.V. (2009) Chemical composition of nyereite and gregoryite from natrocarbonatites of Oldoinyo Lengai volcano, Tanzania. *Geology of Ore Deposits*, 51, 608–616.

MANUSCRIPT RECEIVED MARCH 21, 2021

MANUSCRIPT ACCEPTED NOVEMBER 26, 2021

MANUSCRIPT HANDLED BY DAVID DOLEJS